ISSN: 2634 - 8853

Journal of Engineering and Applied Sciences Technology

SCIENTIFIC Research and Community

Review Article

Open Access

Impact of Water Mist on Heat Transfer and Chemical Species from a Liquid Pool Fire

Sébastien Rivero, Marianne Houndekon, Vincent Robin, Zakaria Bouali, Hernando Maldonado Colman and Hui-Ying Wang*

Pprime Institute (CNRS-UPR 3346, ENSMA, University of Poitiers) Fluid-Thermal-Combustion Department ENSMA – BP 40109 Téléport 2, 1 av. Clément Ader 86961 Futuroscope Chasseneuil Cedex, France

ABSTRACT

The present work provides an experimental and numerical study on suppression phenomena of a buoyant, turbulent heptane medium-scale pool fire via water mist. Detailed gas temperature is presented with and without the addition of a finely divided water mist (50μm). It is found that such mist has a combustion-supporting effect due to upward buoyancy-induced flow opposed to mist injection. The customarily described well defined structure of the flame does not exist any longer by application of water mist. This study evaluated the performance of two widely used fire simulation codes, such as Fire Dynamics Simulator and FireFOAM for predicting pool fire suppression via water mist thanks to the Large Eddy Simulation (LES) technique. The eddy dissipation concept (EDC) is applied to simulations of pool fire suppression, which considers one or three-step chemical reaction. Both simulation codes reasonably predicted the gas temperature trend, and FDS predicts lower temperature stratification in the thermal plume than FireFOAM after activating water mist.

***Corresponding author**

Hui-Ying Wang, Pprime Institute (CNRS-UPR 3346, ENSMA, University of Poitiers) Fluid-Thermal-Combustion Department ENSMA – BP 40109 Téléport 2, 1 av. Clément Ader 86961 Futuroscope Chasseneuil Cedex, France.

Received: May 07, 2026; **Accepted:** May 14, 2026; **Published:** June 11, 2026

Introduction

As an alternative to halogenated alkyl fire extinguishing agents, sprinklers are widely used in industry facilities since it is shown applicable to suppression of gas, liquid and solid combustible fires [1]. Several studies have investigated fire suppression under varying conditions, including compartment configuration, fire size, opening geometry, fuel type, and ventilation effects. During the fire-water interaction period, the fire structure is controlled by water application time, flux density, spray dynamics and droplet size [2-8]. For early application in an environment which is not hot enough to result in a strong droplet evaporation, fuel cooling was identified as the main mechanism leading to fire suppression [3]. Reduction in the flame temperature below a critical value necessary to sustain combustion can be achieved only thanks to activation of fire suppression system at the early stage of fire growth [4]. The fire suppression is significantly affected by airflows produced by natural or forced ventilation in water mist, smoke extraction system and movement of fire load [5]. The fire suppression performance is achieved when droplets evaporate close to the flame sheet via latent cooling effects [6]. Heat radiation from the fire source can be reduced more effectively when the entire fire extinguishing space is filled by the mist via the atomization effect of high-pressure water mist [7]. Suppression performance of turbulent fires via water mist has been investigated without the detailed characterization and controlled conditions necessary for model validation [8].

The effects of radiation modeling and fire suppression strategies like water mist systems have been thoroughly investigated thanks to numerical simulation [9-10]. A widely used computational code in fire modeling is the Fire Dynamics Simulator (FDS) code by using a low-Mach-number approximation to model fluid flow and applying a Large Eddy Smulation (LES) to capture turbulent flame behavior. In addition, the FireFoam code (FM-Global V2306) has recently been increasingly applied to fire simulations. Unlike FDS, FireFoam can handle both compressible and incompressible flows and offers flexibility in modeling turbulent flames using Reynolds-Averaged Navier–Stokes (RANS) or LES techniques. Numerous simulation studies have been conducted by using FDS to explore pool fire dynamics [11-14]. Although FireFoam has been more recently integrated into fire modeling, it has already demonstrated potential in simulating a wide range of compartment fire scenarios. Efforts to enhance FireFoam's modeling capabilities include the development of a Damköhler-number-based flame extinction model, validated through reduced-scale heptane pool fire experiments [15]. Other studies have applied FireFoam to model mechanically ventilated nuclear compartments, incorporating a conjugate heat transfer model to simulate thermal interactions between combustion gases and compartment surfaces [16]. Simulations of large-scale under-ventilated heptane pool fires further demonstrate its applicability to complex fire environments [17]. The research makes a contribution to the field of pool fires and backdraft in a compartment by using both FDS and FireFoam [18]. Both the FDS and FireFoam are widely adopted in fire analysis, and several comparative studies have evaluated their predictive performance thanks to the experimental data. However, the predictive performance is sensitive to factors such as fire conditions, grid resolution, and other simulation parameters.

The results from pool fires suggest that neither code consistently outperforms the other across different fire scenarios. To date, a comparative analysis between FDS and FireFoam for the complex

fire scenario such as fire suppression via water mist is not addressed. The present experimental study shows that interaction between mist and fire leads to a random lateral ejection of premixed flame pockets above an established diffusion flame. The present work must be viewed solely as a diagnostic calculation in fire condition to highlight the importance of working on the developments for droplet aerodynamic modelling including coalescence in dense sprays in both FDS and FireFoam. Developing an effective method to accurately predict the behavior of fire suppression via mater mist is crucial for improving fire prevention and evacuation strategies. The objective of the present work is to provide a detailed experimental and numerical study on fire suppression phenomena via water mist in a buoyant, turbulent diffusion flame. Both the complexity required for relation to realistic fire scenarios and the detailed diagnostics required for validation of CFD tool such as FDS and FireFoam have been contained [11-12].

Experimental Set-Up

Experiments were performed with heptane pool fires, as shown in Fig.1. Heptane was contained in a circular steel pan, 10 cm deep, with a diameter of 23 cm. During the test, the level was kept constant by means of a gravity liquid feeding system based on an electronically controlled on/off valve. The fuel supply rate is 0.66 ± 0.05 g/s.

The water mist system used consists of three nozzles which are located symmetrically with respect to the flame axis (120°) and directed toward the fuel surface centre with an angle of 35°. The distance between the nozzles and the liquid surface is 1.29 m with a radial position 0.7 m. The nozzles are twin fluid (water/air) pressure assisted atomizers permitting the control of the droplet size, flow density, and momentum of the mist. The applied air pressure and water flow are chosen in such a way that complete extinguishment does not occur immediately or even does not occur at all. Each nozzle works at a normal operating air-pressure of 1 bar and provides a water mass flow rate of 3.5 g/s. The local speed, particle size and concentration of the droplet were properly scaled by using a laser anemometry system called PDPA (Phase Doppler Particle Analyser). Water mist is delivered as an opposed buoyancy-induced flow, properly oriented with high momentum, in order to push the water vapour formed against the fuel surface. This allows to analyse in a long duration, on one hand, the perturbation influence of a water mist addition on the interaction between flame destabilization and extinction, and on the other hand, on the radiant heat feedback over the pyrolysis surface. To measure the radiant heat flux over the fuel surface (below 20 kW/m2), three Gardon-gauge-type radiometers Medtherm are used. Each radiometer was water cooled and equipped with a window to eliminate the conductive and convective components from the flame. The window used is in calcium fluoride with a spectral transmittance between 0.3 and 11.5 µm which covers the spectral range of a luminous flame between 0.5 and 5 µm. The view factor of these radiometers was 150° and uncertainty in heat flux measurements is within 3%. The gas temperature was measured with five thermocouple trees type K of chromel-alumel and 0.5 mm wire which are arranged at intervals of 2.5 cm.

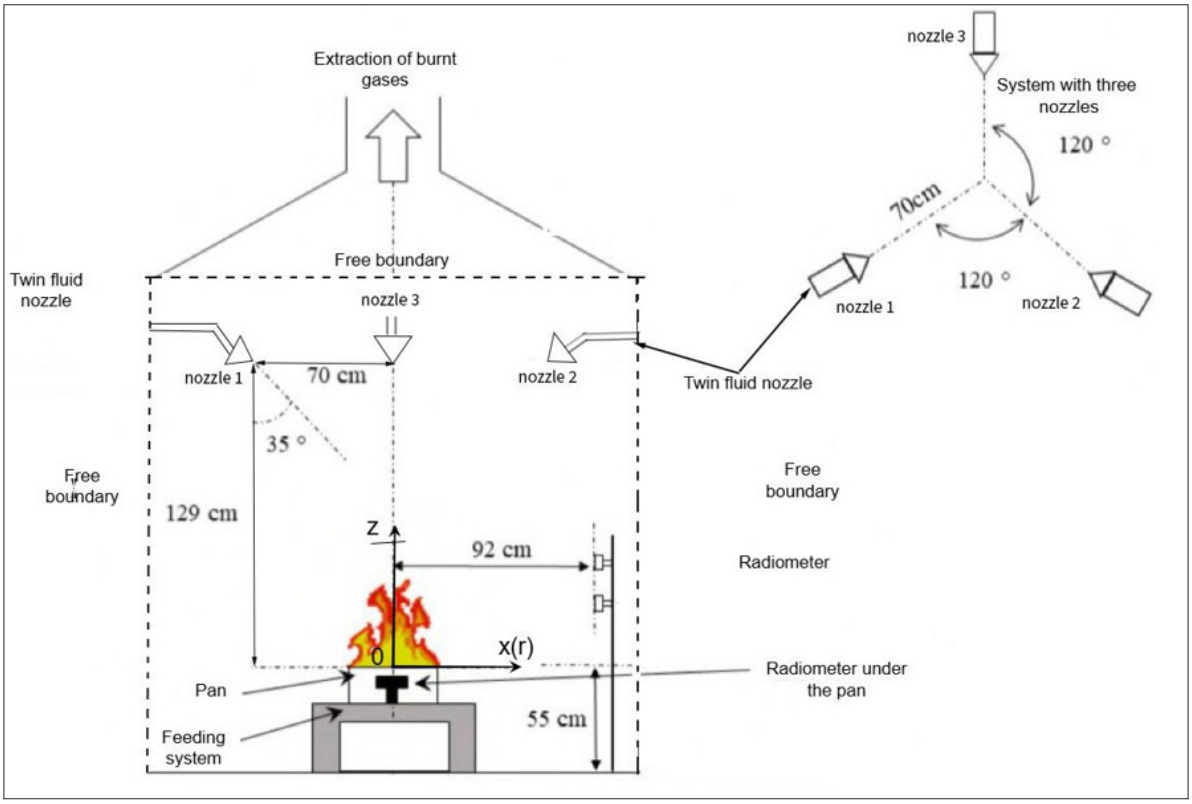

Figure 1: Experimental Set Up with a Water Mist System

Numerical Modelling

Large Eddy Simulation (LES) and the Lagrangian approach are adopted to describe respectively turbulence and water droplet transport. The hydrodynamic model in gas phase consists of the fully three-dimensional, transient equations of mass, momentum, energy and species conservation. For clarity, only the most relevant mathematical models for the present water mist simulation are described here. The governing equations for both the gas and the droplet phases are discretized and iteratively solved, and a detailed description is given in user guide [11-12].

Lagrangian Model

The droplet model such as a Lagrangian approach consists of the droplet evaporation and the rates of change in vapor mass/in the droplet temperature and in the gas temperature.

In the gas phase, the momentum lost from a particle is added to the fluid and vice versa through the drag force.

$$f_b = m_d \mathbf{g} - \frac{1}{2}\rho C_d A_d (\mathbf{u}_d - \mathbf{u})|\mathbf{u}_d - \mathbf{u}|$$

where A_d refers the particle cross-sectional area, u_d the particle velocity, m_d the particle mass, u the gas velocity, ρ the gas density and **g** the gravitational acceleration.

The acceleration of a single spherical droplet is given by

$$\frac{d\mathbf{u}_d}{dt} = g - \frac{1}{2}\frac{\rho C_d A_d}{m_d}(\mathbf{u}_d - \mathbf{u})|\mathbf{u}_d - \mathbf{u}|$$

The parameter C_d in Eqs.(1, 2) represents the drag coefficient between the liquid droplet and the gas, and is a function of the droplet Reynolds number, Re_d.

$$C_d = \begin{cases} 24 Re_d^{-1} & \text{for } Re_d < 1 \\ 24\left(0.85 + 0.15 Re_d^{0.687}\right) Re_d^{-1} & \text{for } 1 < Re_d < 1000 \\ 0.44 & \text{for } Re_d > 1000 \end{cases} \quad (3)$$

$$Re_d = \frac{2 r_d |u_d - u|}{\mu} \quad (4)$$

where r_d is the particle radius and μ the dynamic gas phase viscosity.

In FDS6.8 [11], the drop size distribution is characterized by Cumulative Volume Fraction, which agrees well with a combination of log-normal and Rosin-Rammler distributions.

$$F(d) = \begin{cases} \frac{1}{\sqrt{2\pi}} \int_0^d \frac{1}{\sigma d'} \exp\left(-\frac{[\ln(d'/d_m)]^2}{2\sigma^2}\right) dd' & (d \le d_m) \\ 1 - \exp\left[-0.693 (d/d_m)^\gamma\right] & (d > d_m) \end{cases} \quad (5)$$

where d_m is the median volumetric droplet diameter and γ and σ are empirical constants equal to approximately 2.4 and 0.48, respectively. The droplet diameters are randomly chosen from the given size distribution. The cumulative number fraction, f(d), is

$$f(d) = \frac{F'(d)}{d^3} \Big/ \int_0^\infty \frac{F'(d')}{d'^3} dd' \quad (6)$$

In FireFoam [12], the default drop size distribution models did not adequately represent the spray characteristics observed. Consequently, a custom number probability density function was implemented to directly fit the available experimental measurements taken at a distance of 70 cm from the injection point. It is assumed that the spray is fully developed at this location. Therefore, the distribution is treated as invariant and does not evolve further downstream.

Turbulence model

Following the analysis of Smagorinsky in FDS6.8 [11], the eddy viscosity can be modelled as,

$$\mu_t = C_s^2 \rho \Delta^2 |\bar{S}_{ij}| \quad (7)$$

Here, $|\bar{S}_{ij}|$ is the magnitude of the large scale strain rate tensor, $\bar{S}_{ij}$, $\Delta = (\Delta x \Delta y \Delta z)^{1/3}$ the filter width, and C_S an empirical constant with a standard value of 0.21.

FireFoam [12] simulations employ the k-equation eddy viscosity model for Sub-Grid Scale (SGS) closure. This approach models the energy transfer between resolved and unresolved eddies in LES simulations. The SGS kinetic energy is computed by solving the following transport equation.

$$\frac{\partial \bar{\rho} k_t}{\partial t} + \frac{\partial \bar{\rho} \widetilde{u_j} k_t}{\partial x_j} = \frac{\partial}{\partial x_j}\left(\bar{\rho} D_k \frac{\partial k_t}{\partial x_j}\right) + \bar{\rho} G - \bar{\rho} \varepsilon_t - \frac{2}{3}\bar{\rho}\left(\frac{\partial \widetilde{u_l}}{\partial x_l}\right) k_t + S_k \quad (8)$$

The SGS viscosity is calculated using the following equation:

$$\nu_t = C_k \Delta k_t^{1/2} \quad (9)$$

where the model constant, C_k, is set to 0.094.

Combustion Model

The three-step reaction mechanism, represented by Eqs.(10-12), are employed in the FDS6 simulation [11].

$$C_7H_{16} + 10O_2 \rightarrow 6\ CO_2 + 7\ H_2O + CO + H_2 \quad (10)$$

$$2\ CO + O_2 \overset{H_2O}{\longleftrightarrow} 2\ CO_2 \quad (11)$$

$$2\ H_2 + O_2 \leftrightarrow 2\ H_2O \quad (12)$$

An advanced EDC model is employed for the primitive fuel oxidation (Eq.10) based on a mixing-controlled fast chemistry approach.

$$\dot{\omega}_i''' = \rho\left[\frac{\zeta(t)}{\tau_{mix}}(Y_i - Y_i^0) + (1 - \zeta(t))\frac{dY_i}{dt}\right] \quad \text{and} \quad \zeta(t) = \zeta_0 \exp(-t/\tau_{mix}) \quad (13)$$

where τ_{mix} denotes key mixing timescale, ζ(t) the unmixed fraction at time step t, and the initial value of unmixed fraction, ζ_0 , was set to 1. The rate of change in the mass fraction of species i in the mixed reactor zone, $\frac{dY_i}{dt}$, can be determined by summing the mass rate of the reaction per unit volume for species i across all chemical reactions. Such an EDC (Eq.13) is combined with a finite-rate Arrhenius reverse chemistry to create a mixed reaction. The exothermic reaction of carbon monoxide oxidation and the reversible endothermic reaction of CO_2 (Eq.10) are expressed as follows :

$$\dot{\omega}_{CO}''' = -1.5 \times 10^9 T^0 e^{-41840/RT} [CO][O_2]^{0.25}[H_2O]^{0.5} \quad (14)$$

$$\dot{\omega}_{CO2}''' = -6.16 \times 10^{13} T^{-0.97} e^{-328026/RT} [CO_2][O_2]^{-0.25}[H_2O]^{0.5} \quad (15)$$

The presence of the water vapor in Eqs.(14, 15) is required, but its concentration does not explicitly participate in the reaction. The hydrogen combustion with oxygen is formulated as :

$$\dot{\omega}'''_{H2} = -8.5 \times 10^{15} T^{-1} e^{-167360/RT} [H_2]^{0.25} [O_2]^{1.5} \quad (16)$$

The rate of the corresponding reverse water vapor (H_2O) dissociation is obtained from equilibrium [11].

FireFoam employ the EDM which is based on a simplified one-step global reaction mechanism for fuel.

$$C_7H_{16} + 11O_2 \rightarrow 7CO_2 + 8H_2O \quad (17)$$

Fuel combustion is assumed to be controlled by the turbulent mixing of the fuel and oxidizer, with the chemical reaction occurring instantaneously once the fuel and oxidizer mix at the molecular level. The reaction rate terms for each species i in the species equations can be expressed as:

$$\overline{\omega_f} = \frac{\bar{\rho} \min\left(\widetilde{Y_f}, \frac{\widetilde{Y_{O_2}}}{s}\right)}{c_{stiff} \Delta t} \left(1 - e^{-c_{stiff} \Delta t \, t^{-1}}\right) \quad (18)$$

$$t^{-1} = \max\left(C \frac{\varepsilon_t}{k_t}; C_d \frac{\alpha}{\bar{\rho} \Delta^2}\right) \quad (19)$$

where both the model constants, C and C_d, are set to 4.

Radiation and Soot Models

Radiation Transfer Equation (RTE) is solved with a ray-based method [13] in angular discretization and a finite volume method in spatial discretization. The absorption coefficient in the RTE includes gas-phase radiation of the most important combustion product controlling the thermal radiation, such as H_2O, CO, CO_2, soot and water mist. The more robust Laminar Smoke Point model [19] is implanted in FDS6.8 [11] to calculate soot emission. FireFoam uses a simple soot-yield model.

Heat and Mass Balances at Interface

In FDS6.8 [11], the heat balance is established to calculate the surface temperature of liquid through the convective and radiative heat fluxes. The evaporation rate of liquid fuel is calculated from the Stefan equation [11], as follows :

$$\dot{m}''_F = \frac{\rho D}{L} N_u Ln \left[\frac{1 - Y_{F,g}}{1 - Y_{F,i}}\right] \quad (20)$$

where D denotes the mass diffusivity, L the length scale, $Y_{F,g}$ mass fraction of fuel vapor adjacent to the pyrolysis surface, and Nu Nusselt number. The Clausius–Clapeyron relation is employed in an equilibrium state to find the mass fraction of fuel vapor, $Y_{F,i}$, at the interface as a function of the liquid surface temperature. The measured mass loss rate at the liquid surface is imposed as an input to perform the computation using FireFoam [12]. For both the codes, the mass balance at the burning boundary is established as :

$$\dot{m}''_F = u_n \rho_s Y_{F,s} - (\rho D)_s \frac{Y_{F,g} - Y_{F,i}}{\delta n} \quad (21)$$

where u_n is the normal component of velocity at the surface pointing into the flow domain.

Computational Domain and Boundary Conditions

According to the experimental configuration (Fig.1), the three dimensional computational domain of 2x2x1.6 m3 in the x, y and z directions respectively, is chosen. The grid contains 100x100x150 grid cells, and the finally chosen grid size in an order of 1 cm around the fire source. Indeed, such a mesh size is meaningful only for the calculation of the fluid motion outside the flame zone. An extremely small grid size lower than 1 mm is required to fully resolve turbulent reacting flow instabilities, making practical fire simulations difficult. As shown in Fig.2a, a structured hexahedral grid is employed in FDS [11]. An unstructured mesh using the cylindrical coordinate (Fig.2b) is created by using FireFoam [12], allowing to determine correctly a circular burning surface, and to capture the interaction between the gas flow and the cylinder edges. The liquid surface is 23 cm in diameter and is embedded in the z=0 plane, centered in the x, and y directions. Zero gradient conditions are used for the far-field free boundary values of the variables.

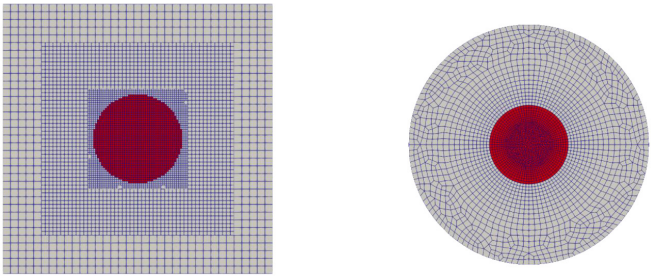

a) Structured mesh in FDS6 b) Unstructured mesh in FireFoam

Figure 2: Three dimensional computational domain and mesh distribution

Results and Discussions

Non-fire tests involving only water spray from one nozzle were carried out to calibrate the volume-median diameter used in FDS6 at the nozzle exit. At a distance of 70 cm from the nozzle exit, droplet Sauter Mean Diameter and an injection velocity of water mist were experimentally determined. Thanks to the comparison with the experimental data in Figs.(3, 4), a droplet diameter of about D=50µm and an injection velocity of U=10 m/s at the nozzle exit are chosen as an input to perform the computation by using FDS6.8 [11]. The measured local speed and Sauter Mean Diameter at a distance of 70 cm from the nozzle exit are imposed by using FireFoam due to lack of the drop size distribution model (Eqs.5, 6) [12].

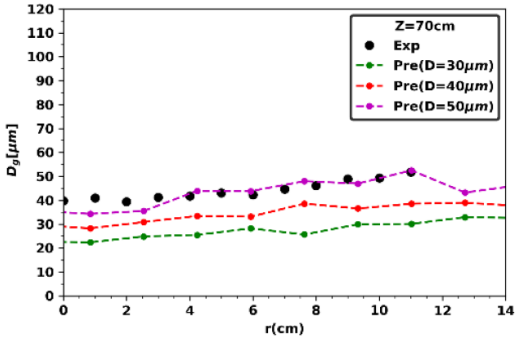

Figure 3: calibration of Sauter Mean Diameter

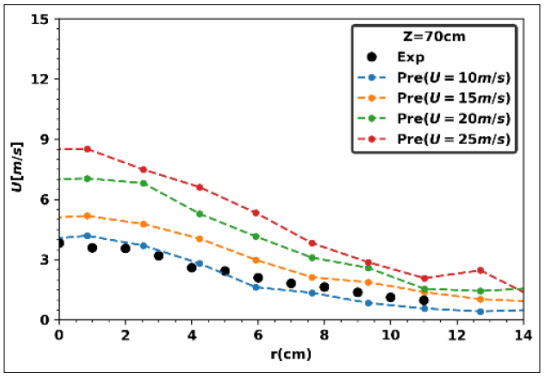

Figure 4: Calibration of mist injection velocity

In no water mist case, both the experiment (Fig.5c) and the prediction (Fig.5a, b) show that the overall time-averaged temperature distributions are well characteristic of those encountered in diffusion flames. The distributions of temperature obtained from FireFoam and FDS6 showed similar trends with a maximum temperature at the edge indicating the presence of high reactivity. One significant difference is that the FireFoam results show the thermal plume layer maintaining an elevated temperature (1700°C), whereas the FDS6 results do not exhibit such a high-temperature core distribution near the pool edge.

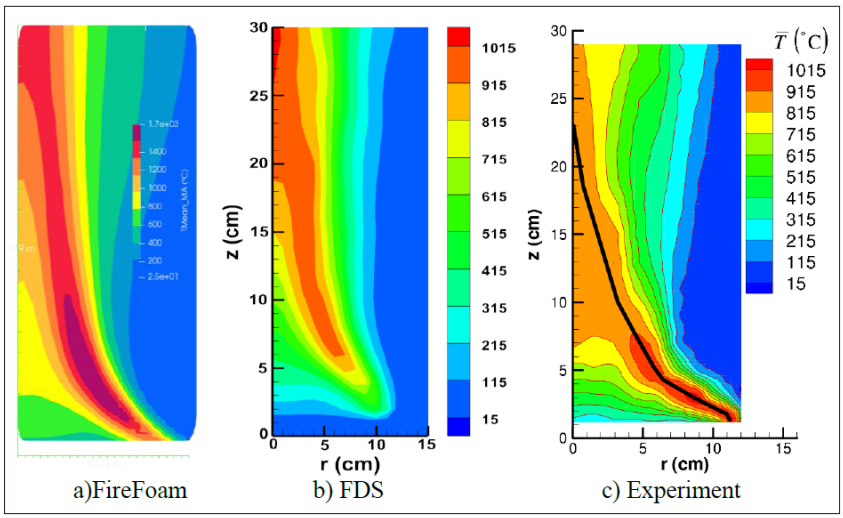

Figure 5: Distribution of The Predicted and Measured Time-Averaged Temperature in No Water Mist Case

Fig.6(a, b) compares the profiles in temperature predictions from FireFoam and FDS6 with experimental measurements along the flame axis at the five radial positions (r=0, 3, 6, 9 and 10.5 cm) before activation of water mist. Overall, FireFoam and FDS6 results showed a similar tendency observed in the experiments. As compared to the measured gas temperature, there is only a good prediction at r=0 cm using FireFoam and at r=6 cm using FDS6 along the flame axis. At the front locations of the edge (r=9, 10.5 cm), the gas temperatures are significantly lower owing to dilution by the stronger buoyancy-induced air at the flame base. Overall, FireFoam tends to overpredict the experimental values, whereas FDS6 to predict significantly lower temperatures than FireFoam, aligning more closely with the experimental data.

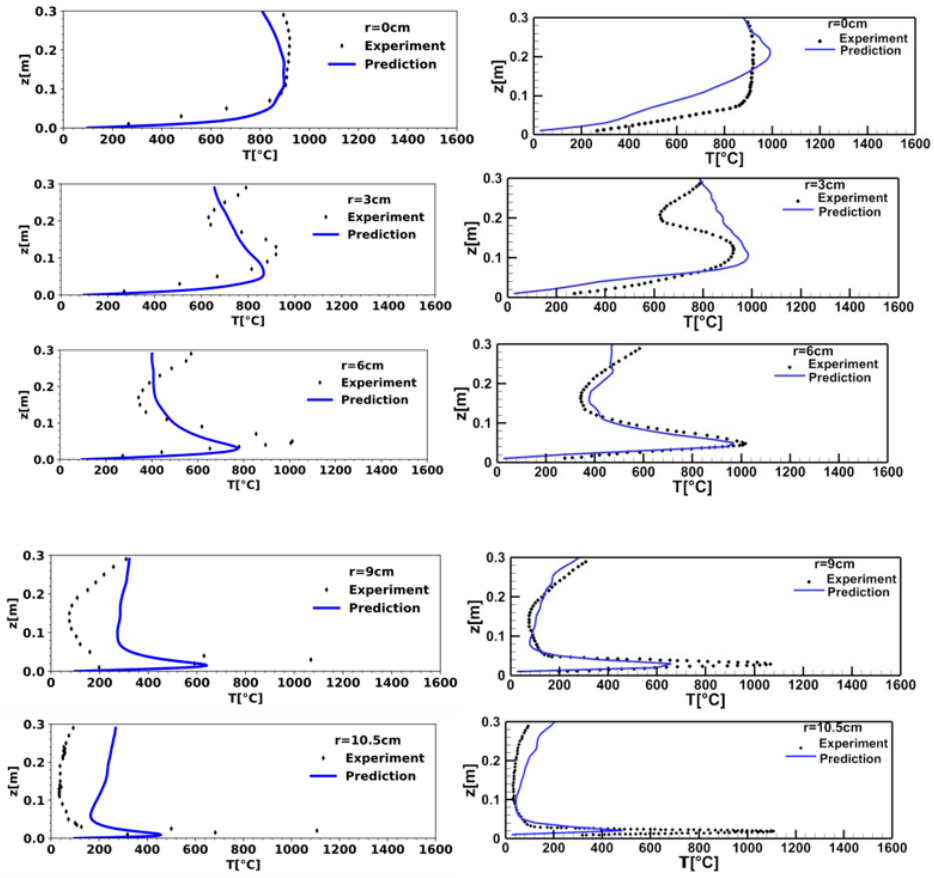

a) FireFoam b) FDS6

Figure 6: Comparison of Predicted and Measured Axial Temperature Along The Five Thermocouple Trees in No Mist Case

Qualitative instantaneous images from a CCD camera are presented in Fig.7(a, b, c). The time-varying visible flame oscillation is characterized by a flame necking phenomenon and the intermittent zone. Addition of water vapor at t0=60 s into a flame has a combustion-supporting effect. This results in a total destruction of the flame at t=t0+5 s with the two competing effects such as a random lateral ejection of premixed flame pockets and an established diffusion flame. The droplets disturb the turbulent flame structure with the occasional wisp of flame at the top of the reactive zone that escape the water mist cloud. Application of water mist precedes only partial fire extinguishment at t=t0+10 s with a reduction in the flame size.

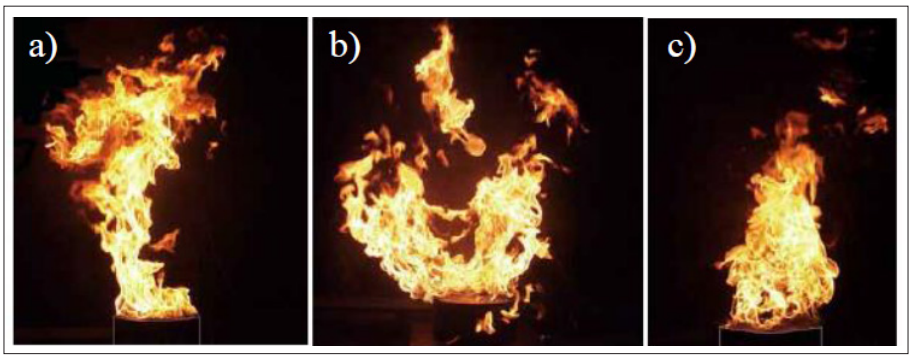

Figure 7: Instantaneous Flame Images During Interaction Between Fire and Water Mist with Application Time At t0=60 s (a), t=t0+5 s (b) and t=t0+10 s (c)

As shown in Fig.7, after application of water mist, mixing and reaction processes are random in time and space and the distinction between rich and lean regions becomes ill-defined. Therefore, time-averaged temperature field from the instantaneous flame structure (Fig.7), as that obtained in Fig.8c, cannot be expected to give deeper insight into the detailed mechanisms. Under conditions of water vapour addition, the measured maximum temperature is moved toward the pyrolysis surface partly due to a water–gas shift reaction. It is worth noting that the general characteristics of the predicted evolutions using both the two codes are in qualitative agreement with the measured flame structure with a reduction in temperature level. These results indicate that FDS6 tends to under-predict the flame zone with a visual similarity compared to the measured flame structure, while FireFoam to overpredict the flame zone. Although the validation

of the temperature fields is just qualitative, it does provide a good indication of the impact of the mist on the macroscopic variables of the process, such as the thermal field regardless of the code used.

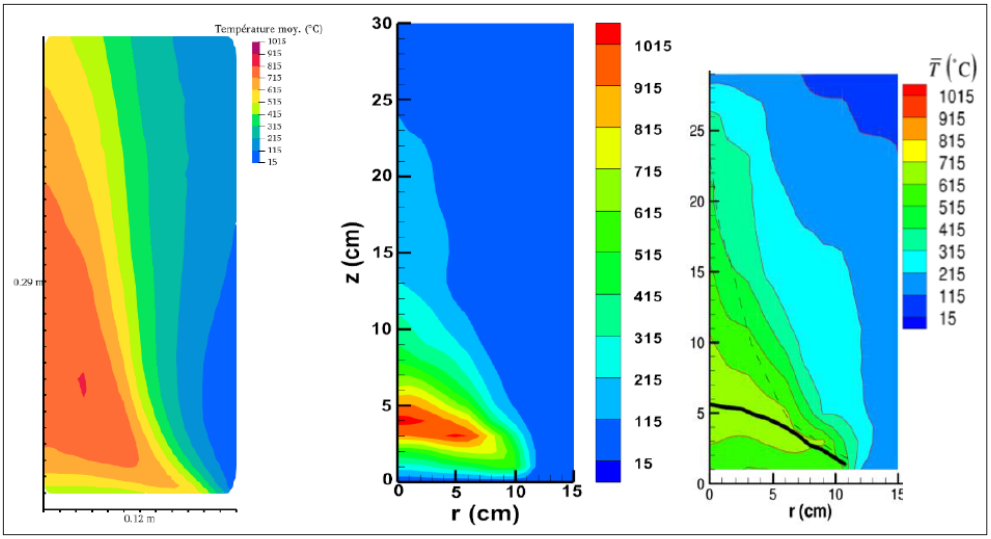

a) FireFoam b) FDS6 c) Experiment

Figure 8: Measured (a) and predicted (b) time-averaged temperature distribution after activation of water mist

Profiles of the predicted axial temperature using FireFoam and FDS6 are compared to the measured ones in Fig.9(a, b) at the five locations (r=0, 3, 6, 9 and 10.5 cm) along the axis after application of water mist. Both the prediction and experiment show that a consecutive efficient cooling of the thermal plume via water mist cannot reduce the flame temperature below a critical temperature of 400°C necessary to sustain combustion. The temperature magnitude depends on both the flame radiation due to the increase of water vapour concentration within the flame, and the decrease due to less soot formation. FireFoam predicts the thermal plume tip to be higher than the experimental data, but it accurately and reasonably predicts the temperature peak and the location it occurs. In contrast, FDS6 predicts the temperature peak that is significantly higher than the experimental values, and underpredicts the full thermal plume tip, reflecting less intense flame propagation after droplet evaporation. Considering these results, it can be confirmed that inside the water mist cloud, FireFoam induces a more intense progression of combustion, and these trends reflect a progressive decrease in temperature.

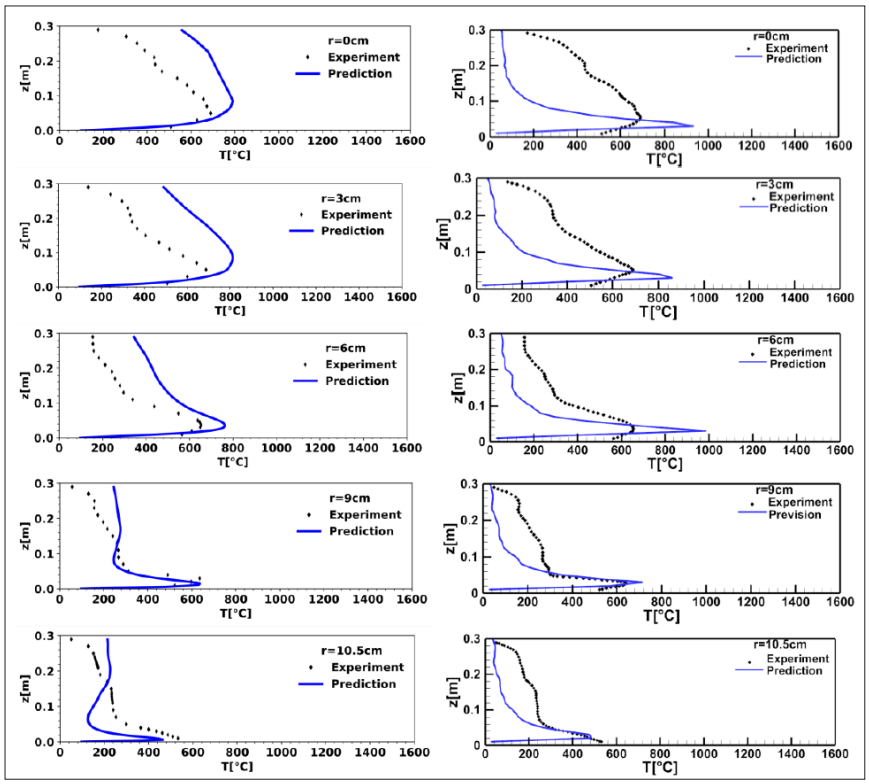

a) FireFoam b) FDS6

Figure 9: Comparison of Predicted and Measured Axial Temperature Along The Five Thermocouple Trees After Activation of Water Mist

In FDS6.8, the heat balance is established to calculate pyrolysis rate over heptane surface, as shown in Fig.10, to supply a permanently burning flame [11]. The expansion effect of the water vapour shifts the region of high temperature towards the burning surface, and an enhancement of the burning rate is related to the significance of convective heat flux after application of water mist. The pyrolysis rate remains uniform over the burning surface except with a sharp decrease near the edge of the pool fire due to a decreasing trend of the liquid temperature. The resulting radiant emission from the flame which in turn determines the burning rate, is shown in Fig.11. The radiative flux is a temperature-sensitive volumetric mechanism associated with both the gas temperature and concentration of emitting species as CO_2, H_2O and soot. The radiation heat flux gives a peak in heat flux of about 15 kW/m^2 in no mist case. A high radiative heat flux covers the entire pyrolysis area because a larger flame zone yields substantial soot and luminous radiation. Application of water mist conducts to a decrease of radiative heat flux to 10 kW/m2 due to reduction in the flame volume. The deviation of the FDS6 results in relation to the measured radiative heat flux is within 50% mainly due to the worse prediction of the gas temperature around the fire source (Fig.9).

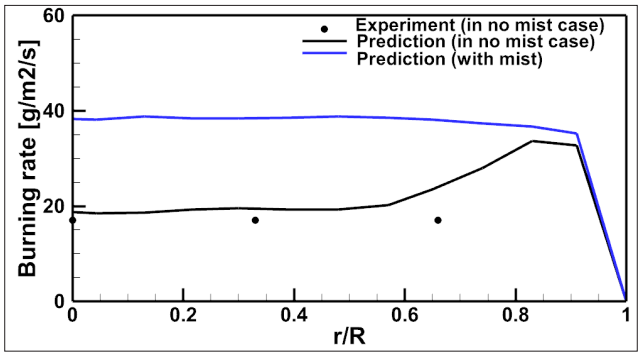

Figure 10: Evolution of The Pyrolysis Rate Along the Burning Surface Before and After Application of Water Mist

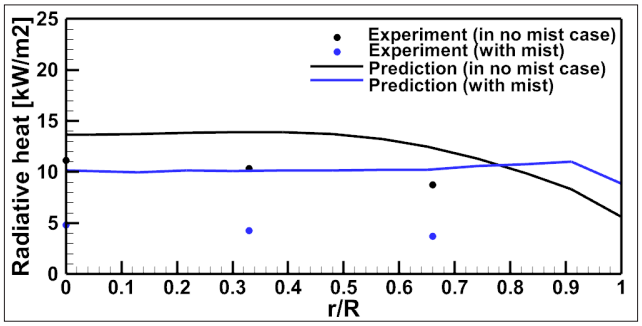

Figure 11: Evolution of The Radiation Heat Flux Over the Pyrolysis Surface Before and After Application of Water Mist

A typical example using FDS6 of the predicted distribution of the combustion products such as carbon monoxide, hydrogen and soot on the symmetrical plane (x, z) is presented in Figs.12 and 13(a, b, c). In no mist case (Fig.12), the buoyancy-induced flow carries abundant combustion products along the forward flow with a slow decay of the toxic emission. After application of mist, the flame allows to entrain more water vapour which is capable of providing a quick decay of the toxic emission in a thermal plume region, as shown in Fig.13. It seems that the peak in CO and hydrogen molar fraction is weakly dependent on water mist with a maximum of roughly 1% which is indicative of an equivalent fuel-air ratio in the reaction region. The interpretation from the FDS6 results can only be of qualitative and speculative nature due to lack of measurements of chemical species in the flame. In addition, there are rather complex combinations of mixing and reaction processes with water mist addition, neither of which are stationary in space and time. It is worth noting that H2 is highly flammable with an ignition energy that is smaller than that of CO and soot [4]. In no mist case, the majority of soot emission (Fig.12c) takes place downstream in the fuel-rich core where heat is released as the fuel reacts with the entrained air. After activation of water mist, soot peak (Fig.12c) is reduced by a factor of two, and the majority of soot formation occurs at the bottom of the fire. Globally, application of water mist significantly reduces the extent of combustion products due to an efficient dilution via droplet evaporation.

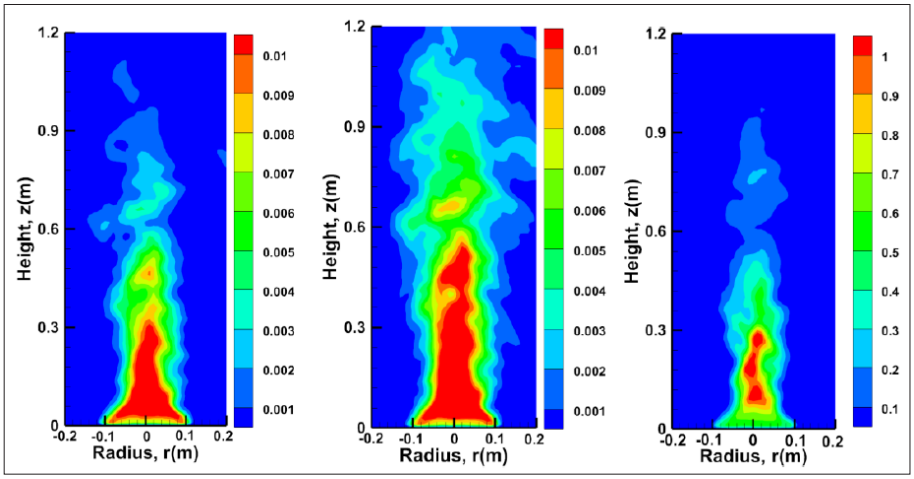

a) Carbon monoxide b) Hydrogen c) Soot

Figure 12: Distribution of The Predicted Co, H2 and Soot Concentration (Mol/Mol) in No Mist Case

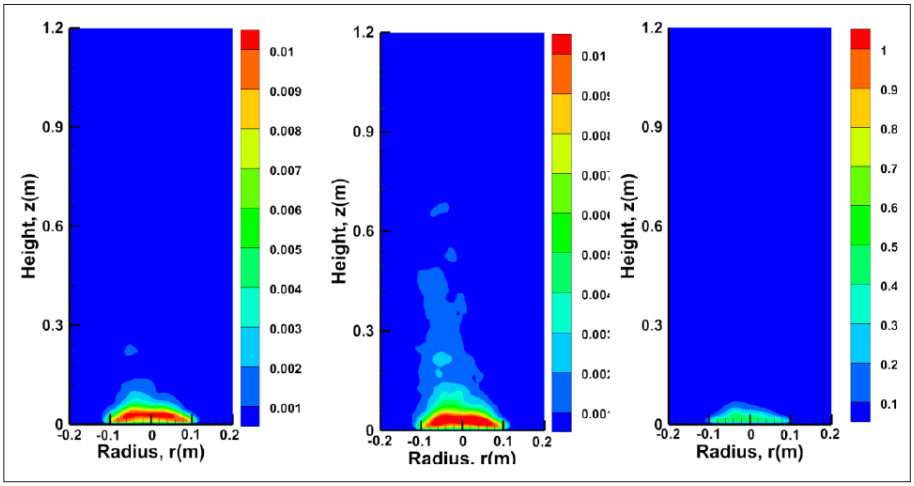

a) Carbon monoxide b) Hydrogen c) Soot

Figure 13: Distributioan) of The Predicted Co, H_2 and Soot Concentrations (Mol/Mol) After Application of Water Mist

Conclusions

In this study, simulations were conducted using FireFoam and FDS to assess their predictive capabilities for the suppression of a turbulent diffusion flame by applying water mist. Both FireFoam and FDS demonstrated reasonable accuracy in predicting the impact of water mist on the temperature field in the heptane pool fire scenario. While FDS6 predicts higher temperature peak than FireFoam, both tools are able to capture the experimental trends effectively. FireFoam provided more accurate prediction for temperature peak at specific positions within the mist cloud, though both simulation tools are in relatively good alignment with the experimental data. FireFoam also provided a more reasonable representation of the temperature distribution along.

the flame axis, whereas FDS, despite predicting higher temperature peak, showed a less pronounced flame distribution. The findings provide valuable insights into the relative performance of FireFoam and FDS for modeling complex fire scenarios, each excelling in different aspects. This study contributes to the understanding of the comparative strengths of these simulation tools and their respective applications in fire suppresion research.

Future work could explore the potential benefits of refining both tools for larger, more complex environments could help improve their predictive capabilities in diverse fire dynamics contexts. Moreover, in order to clarify the chemical effect of water vapour on diffusion flame, OH* or other radical measurements or prediction should be of particular importance. An improved prediction of the two competing effects such as premixed and diffusion flames in presence of water mist, emphasizes the need for developing advanced numerical models including a detailed heptane-air chemical reaction mechanism. The future study aims to calls upon new developments for droplet aerodynamic modelling in water mist sprays in both the FireFoam and FDS6 codes because of the perturbing influence of the injected water mist inside the flame.

References

1. Liu Y, Wang X, Liu T, Ma J, Li G, et al. (2020) Preliminary study on extinguishing shielded fire with water mist. Process Saf. Environ. Prot 141: 344-354.
2. Liu Z, Kim AK (2000) Review of water mist fire suppression systems-fundamental studies. J. Fire Prot. Eng 10: 32-50.
3. Jenft A, Boulet AP, Collin A, Trevisan N, Mauger PN, et al. (2017) Modeling of fire suppression by fuel cooling. Fire Saf. J 91: 680-687.
4. Grant G, Brenton J, Drysdale D (2000) Fire suppression by water sprays. Prog. Energy Combust. Sci 26: 79-130.

5. White JP, Verma S, Keller E, Hao A, Trouvé A, et al. (2017) Water mist suppression of a turbulent line fire. Fire Saf. J 91: 705-713.
6. Liu Y, Fu Z, Zheng G, Chen P (2022) Study on the effect of mist flux on water mist fire extinguishing. Fire Saf. J 130: 103601.
7. Yao Y, Li YZ, Ingason H, Cheng X, Zhang H (2020) Theoretical and numerical study on influence of wind on mass loss rates of heptane pool fires at different scales. Fire Saf. J 120: 103048.
8. Ingason H, Li YZ (2019) Large scale tunnel fire tests with different types of large droplet fixed fire-fighting systems. Fire Saf. J 107: 29-43.
9. Maragkos G, Merci B (2024) Influence of radiation modelling in under-resolved FDS free-burn simulations. Int. J. Heat Fluid Flow 107: 109437.
10. Dasgotra A, Rangarajan G, Tauseef SM (2021) CFD-based study and analysis on the effectiveness of water mist in interacting pool fire suppression. Process Saf. Environ. Prot 152: 614-629.
11. Fire Dynamics Simulator (FDS) and Smokeview (SMV) (2025) https://pages.nist.gov/fds-smv.
12. OpenFOAM documentation (2025) https://www.openfoam.com/documentation/guides/latest/doc/guide-applications-solvers-combustion-fireFoam.html.
13. Hwang CH, Lock A, Bundy M, Johnsson E, Ko GH (2010) Studies on fire characteristics in over- and under-ventilated full-scale compartments. Int. J. Fire Sci.28: 459-486.
14. Vilfayeau S, Ren N, Wang Y, Trouvé A (2015) Numerical simulation of under-ventilated liquid-fueled compartment fires with flame extinction and thermally-driven fuel evaporation. Proc. Combust. Inst 35: 2563-2571.
15. Vilfayeau S, Ren N, Wang Y, Trouvé A (2015) Numerical simulation of under-ventilated liquid-fueled compartment fires with flame extinction and thermally-driven fuel evaporation. Proc. Combust. Inst 35: 2563-2571.
16. Ukairo O, Dembele S, Heidari A, Pretrel H, Wen J (2021) Investigation of fires in a mechanically ventilated compartment using the CFD code FireFOAM. Nucl. Eng. Des 384: 111515.
17. Cavazzuti M, Tartarini P (2024) Pool fires within a large under-ventilated environment: experimental analysis and numerical simulation using OpenFOAM. Fire Techno 60: 1891-1915.
18. Myilsamy D, Oh CB, Jeon J (2025) Large eddy simulations of pool fires and backdraft in a compartment using FDS and FireFOAM. Case Stud. Therm. Eng. 72: 106337.
19. Yao W, Zhang JP, Nadjai A, Beji T, Delichatsios MA (2011) A global soot model developed for fires: validation in laminar flames and application in turbulent pool fires. Fire Saf. J 7: 371-387.